Electronic Supplementary Material (ESI) for Journal of Materials Chemistry A.
This journal is © The Royal Society of Chemistry 2021

Supporting Information

Photo-charge regulation of metal-free photocatalyst by carbon dots for efficient and stable hydrogen peroxide production

Yi Li [a], Yu Zhao [b], Jie Wu [a], Yidong Han [a], Hui Huang [a], Yang Liu [a,*], and Zhenhui Kang [a,c,*]

[a] Institute of Functional Nano and Soft Materials (FUNSOM), Jiangsu Key Laboratory for Carbon-based Functional Materials and Devices, Soochow University, Suzhou 215123, China.

[b] Department of Information Technology, Suzhou Institute of Trade & Commerce, 287 Xuefu Road, Suzhou, 215009, Jiangsu, China.

[c] Macao Institute of Materials Science and Engineering, Macau University of Science and Technology, Taipa, Macau SAR 999078, China.

*Correspondence to: yangl@suda.edu.cn; zhkang@suda.edu.cn

Supplementary Text

S1. Element contents of $CN_{1.8}$/ICT/CDs composite

The elemental analysis of C, N, O, H and S in $CN_{1.8}$/ICT/CDs measured by combustion method has been listed as follows:

Table S1. The element contents of C, N, O, H and S in $CN_{1.8}$/ICT/CDs.

Element	Wt.%
C	55.00
N	33.65
O	8.01
H	3.32
S	0.02
Total:	100.00

S2. Calculation process of valence band (VB) determined by UPS

The valence band energy (E_{VB}) can be determined according to the following equation (2):

$$E_{VB} = -\left(21.22 - \left(E_{cutoff} - E_{fermi}\right)\right) eV \quad (2)$$

where 21.22 eV is the emission energy of Helium irradiation, E_{cutoff} is the cut-off binding energy, E_{fermi} is the energy difference between Femi level (E_F) and the valence band maximum (E_{VB}). The E_{cutoff} and E_{fermi} can be extrapolated from the linear part interception to x-axis.

S3. Apparent quantum efficiency (AQE) calculations.

The apparent quantum efficiency can be evaluated from equation:

$$AQE = \frac{2 \times n_{H_2O_2} \times N_A}{N} \quad (3)$$

N_A is the number of evolved H_2O_2 molecules, is avogadro number (6.02×10^{23}) and N represents the number of incident photons, which can be calculated from the following equation:

$$N = \frac{light\ intensity\ (W\ cm^{-2}) \times illumination\ area\ (cm^2) \times illu}{\frac{hc}{\lambda}} \quad (4)$$

h is plank constant (6.626×10^{-34} J·s = 4.136×10^{-15} eV·s), c is the speed of light (3.0×10^{8} m·s^{-1}), λ is the wavelength of light (365, 420, 485, 595 and 630 nm). The photocatalytic systems with 8 mg catalyst and 15 mL water were irradiated for 6 h at room temperature and atmospheric pressure, without any sacrificial reagents. The irradiated area is 9.0746 cm^2.

S4. Determination of solar-to-chemical conversion (SCC) efficiency.

The free energy for H_2O_2 formation:

$$H_2O + \frac{1}{2}O_2 \rightarrow H_2O_2 \left(\Delta G = 117\ kJ\ mol^{-1}\right) \tag{5}$$

The total input energy:

$$E_{solar}\,(W) = irradiance\ \left(W\ cm^{-2}\right)\ \times\ irradiated\ area\ (cm^2) \tag{6}$$

The determination of SCC:

$$SCC\ efficiency\ (\%) = \frac{\left[\Delta G\ for\ H_2O_2\ generation\ \left(J\ mol^{-1}\right)\right]\ \times\ [H_2O_2\ fromed\ (mol}{[total\ input\ energy\ (W)]\ \times\ [reaction\ time\ (s)]} \tag{7}$$

According to equation (5), the free energy for H_2O_2 generation is 117 kJ·mol^{-1}. The irradiance of simulated solar source is 29.55 mW·cm^{-2}, while the irradiated area is 9.0746 cm^2. The reaction time is 6 h, and the amount of H_2O_2 generated in 15 mL solution with 8 mg catalyst is 111.78 μmol. On the whole, according to equation (6) and (7), SCC efficiency can be calculated to be 0.23%.

S5. The transient photovoltage (TPV) measurements.

The TPV measurements were conducted under room temperature on platinum net covered with powder sample (1cm×1cm) as the working electrodes and Pt wire as the counter electrodes. The *in-situ* TPV were carried out under room temperature with indium-tin oxide (ITO) glass (1cm×2cm) as the working electrodes and Pt wire as the counter electrodes. The working electrodes were prepared by depositing samples (100 μL, 2 $mg \cdot mL^{-1}$, dispersion liquid: 79.5% water, 20% isopropanol and 0.5% Nafion solution(v/v), respectively) on ITO glass substrates. During the testing process, the working electrodes were kept wet with anhydrous acetonitrile (or adding H_2O, N_2, O_2 saturated). The samples were excited by a laser radiation pulse (λ=355 nm, pulse width 5 ns) from a third-harmonic Nd: YAG laser (Polaris II, New Wave Research, Inc.). The photocurrent is the ratio of the photovoltage to the internal resistance of the test systems.

S6. Calculation process of average recombination lifetime (τ_{avg}) in TPV curves.

Single exponential fit of time decay constant:

$$y = C_1 e^{-\frac{x}{\tau 1}} + y_0 \quad (8)$$

C_1 is the fitting undetermined coefficient, τ_1 is time decay constant in charge recombination process, y_0 is constant term.

The formula for calculating average recombination lifetime:

$$\tau_{avg} = \frac{C_1 {\tau_1}^2 + C_2 {\tau_2}^2}{C_1 \tau_1 + C_2 \tau_2} \quad (9)$$

According to equation (7) and (8), the calculation results are shown in Table S1:

Table S2. The average recombination lifetime of each catalyst

	C_1	τ	C_2	τ'	τ_{avg}
$CN_{1.8}$	80.041	0.582	/	/	0.582
ICT	4043.426	0.338	0.117	28.81	0.408
$CN_{1.8}$/ICT	439.727	0.451	0.122	7.938	0.487
$CN_{1.8}$/CDs	2821.456	0.417	/	/	0.417
ICT/CDs	380.071	0.496	0.321	6.682	0.565
$CN_{1.8}$/ICT/CDs	1950.884	0.372	0.178	3.995	0.376

S7. The measurement of electron transfer number.

The rotating disk-ring electrode (RRDE) collection experiments were carried out in N_2-purged Na_2SO_4 solution (0.1 M). 6.3 μL catalyst solution (5 mg mL^{-1}) was dropped onto the surface of RRDE electrode as the working electrode. The $Hg/HgCl_2$ electrode and carbon rod electrode were used as reference electrode and counter electrode, respectively. The rotating speed was 1600 rpm. The electron transfer number was derived from the following equation (10):

$$n = \frac{4\Delta I_{disk}}{\Delta I_{disk} + \Delta I_{ring}/N} \qquad (10)$$

where ΔI_{disk} and ΔI_{ring} are the difference of disk current density and ring current density between darkness and light, respectively. As the RRDE collection efficiency, N was experimentally determined to be 0.37, and it referred to the fraction of H_2O_2 formed at the disk that was collected at the ring. The disk potential was set at open circuit voltage, and the ring potential was set at 0.9 V vs. SCE to detect H_2O_2 generation. According to equation (10), the n value of the water oxidation reaction was calculated to be 2.34.

S8. Experiment of photocatalysis

First, 8 mg of catalyst was added to a 45 mL transparent glass bottle. Then add 15 mL of ultrapure water to the bottle, seal the mouth of the bottle with a rubber stopper and squeeze it with an aluminium plastic cap. Then place the mixture in the glass bottle under ultrasound dispersed uniformly in the instrument. Finally, the reaction was performed under visible light ($\lambda \geq 420$ nm) for 120 h. The suspension was centrifuged to remove the photocatalyst. The H_2O_2 produced by the reaction was added with a 1mL H_2SO_4 solution (3mol L^{-1}). The acidic $KMnO_4$ reagent solution (0.01mol L^{-1}) was subjected to redox titration. When the solution became pink after the addition of $KMnO_4$ solution and the colour of the solution was kept for 1 min, the concentration of $KMnO_4$ solution was used to calculate the concentration of H_2O_2.

S9. Characterization

The scanning electron microscope (SEM), transmission electron microscopy (TEM) and energy dispersive X-ray (EDX) spectroscopy were acquired from a FEI-Quanta 200 FEG scanning electron microscope and FEI-Tecnai F20 transmission electron microscope (200 kV). The crystal structure of samples was examined by a PIXcel3D X-ray diffractometer (Empyrean, Holland Panalytical) with Cu Kα radiation (λ = 0.15406 nm). Fourier transform infrared (FTIR) spectrum was recorded on a FTIR spectrometer over the scan range of 400-4000 cm^{-1}, using a standard KBr pellet technique. Raman spectra were collected by using a HR 800 Raman spectroscope (J Y, France) with a 20 mW air-cooled argonion laser (633 nm) as the excitation source. X-ray photoelectron spectroscopy (XPS) measurements were performed by an Escalab 250Xi X-ray photo-electron spectroscope (Thermo Fisher Scientific, America). Ultraviolet photoelectron spectroscopy (UPS) measurements were carried out with He I (21.22 eV) as the monochromatic light source. Room temperature UV-Vis adsorption spectrum was caried out from a UV/VIS/NIR spectrophotometer (Lambda 750, Perkinelmer). Electron spin-resonance spectroscopy (ESR) measurements were performed by an ESR spectrometer (Bruker A300). Electro-catalysis measurement was acquired from a Model CHI 760C workstation (CH Instrument, Shanghai, China). The PL study was implemented on a Horiba Jobin Y von (Fluoro Max4) Lumines cence Spectrometer.The contact angle measurements were carried out using a Dat aPhysics OCA contact-angle analyzer (DataPhysics, Germany). The 1H nuclear magnetic resonance spectroscopy was detected by Bruker AVANCEAV III 400. Elemental analysis was tested by elementar Micro cube and elementar EL III.

Supplementary Figures.

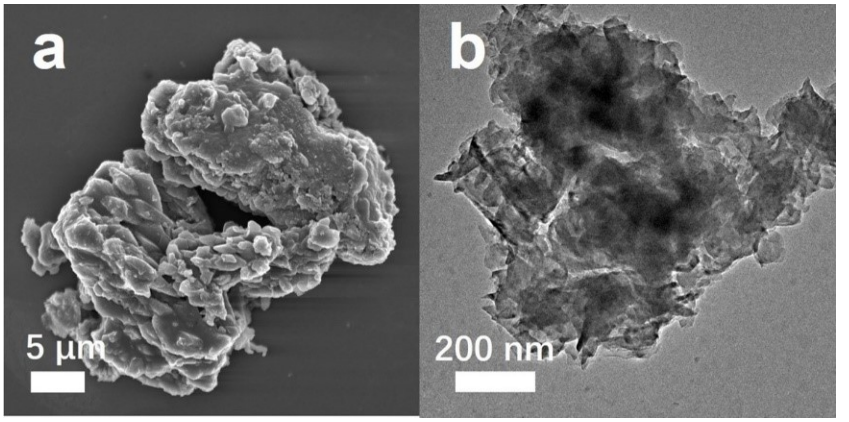

Figure S1. (a) SEM and (b) TEM images of bulk $CN_{1.5}$.

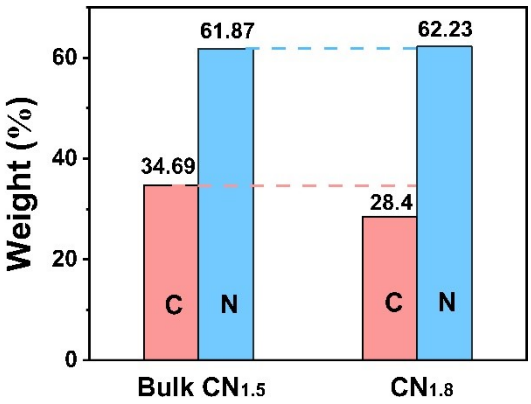

Figure S2. Elemental analysis of C, N in bulk $CN_{1.5}$ and $CN_{1.8}$.

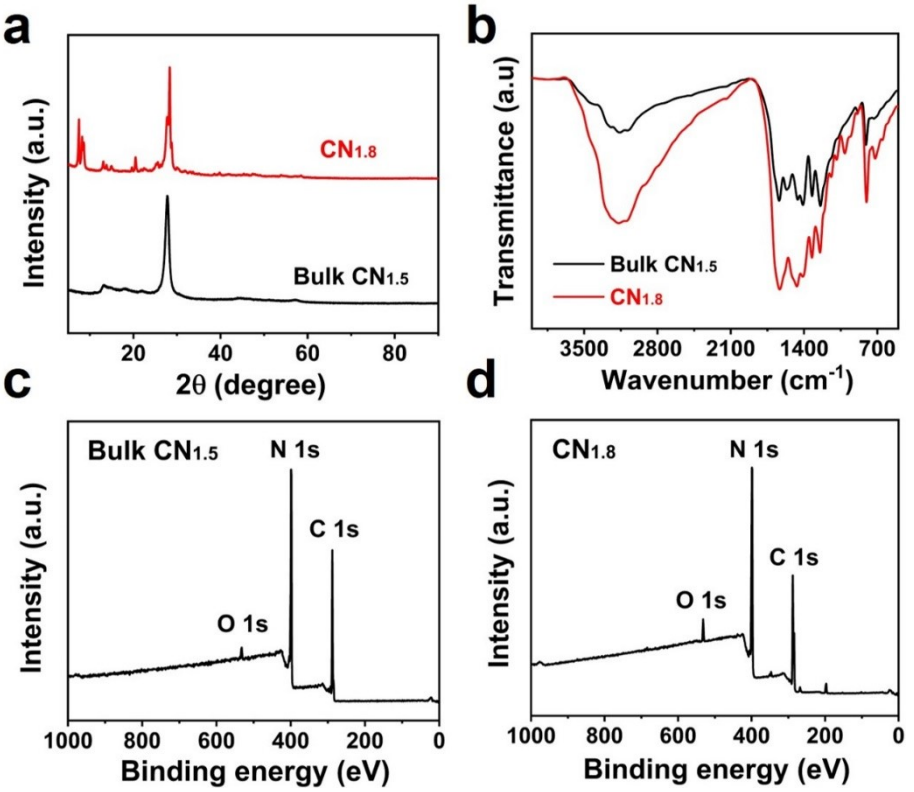

Figure S3. (a) XRD patterns and (b) FTIR spectra of $CN_{1.8}$ (red line) and bulk $CN_{1.5}$ (black line), XPS survey spectrum of (c) bulk $CN_{1.5}$ and (d) $CN_{1.8}$.

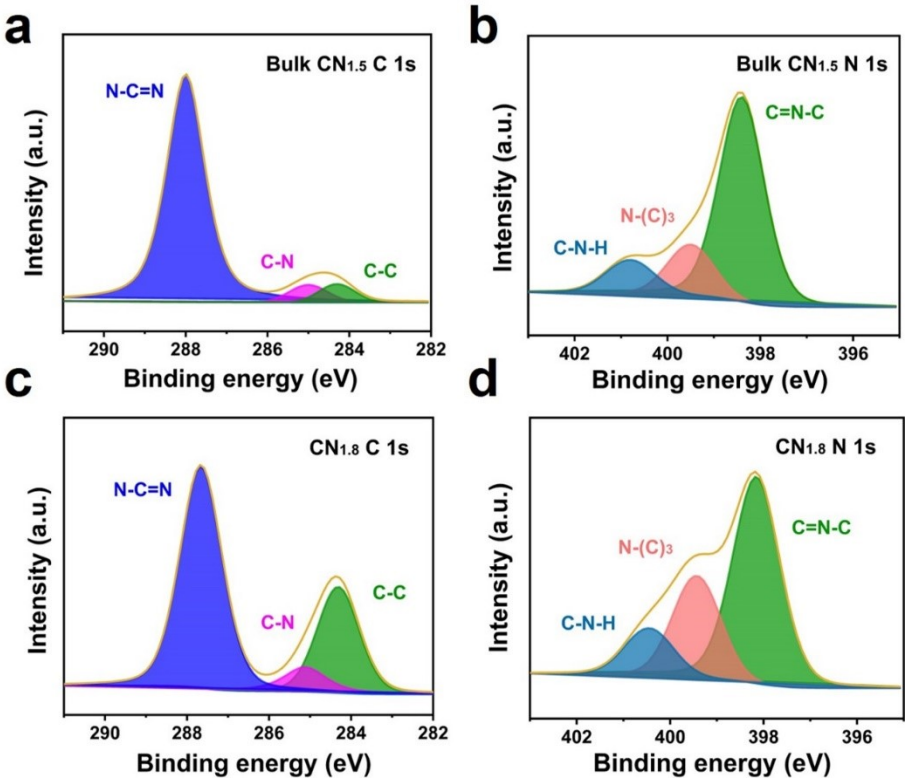

Figure S4. High-resolution XPS spectra of bulk $CN_{1.5}$: (a) C 1s, (b) N 1s and high-resolution XPS spectra of $CN_{1.8}$: (c) C 1s, (d) N 1s.

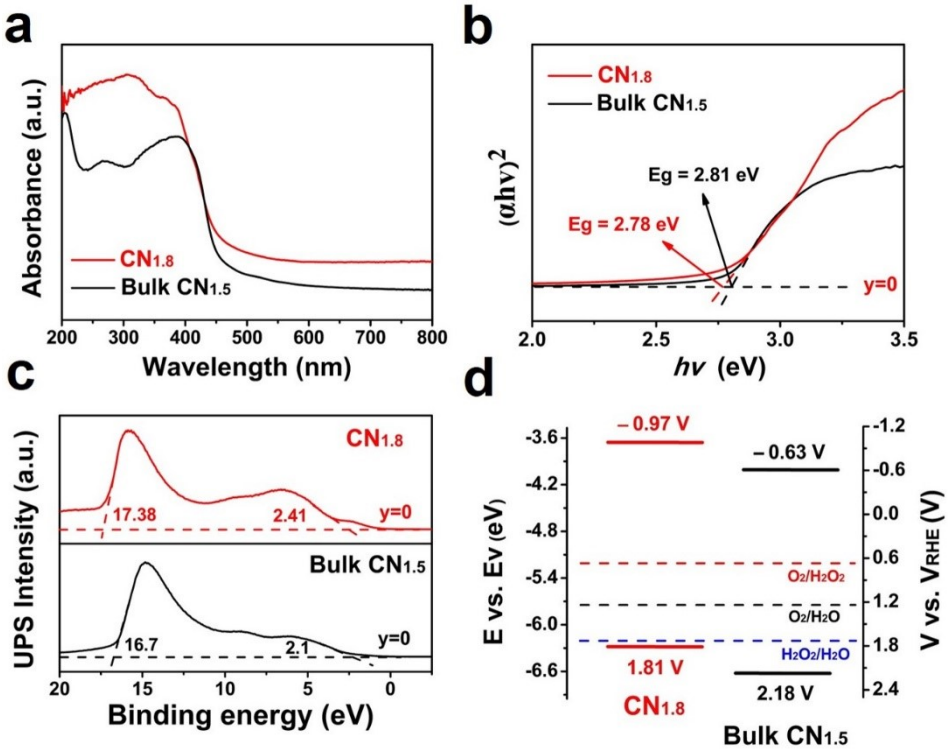

Figure S5. (a) UV-vis absorption spectra of $CN_{1.8}$ and bulk $CN_{1.5}$. (b) Plots of $(\alpha h\nu)^2$ versus energy ($h\nu$) for $CN_{1.8}$ and bulk $CN_{1.5}$. (c) UPS spectrum of $CN_{1.8}$ and bulk $CN_{1.5}$. (d) Band structure diagram of $CN_{1.8}$ and bulk $CN_{1.5}$.

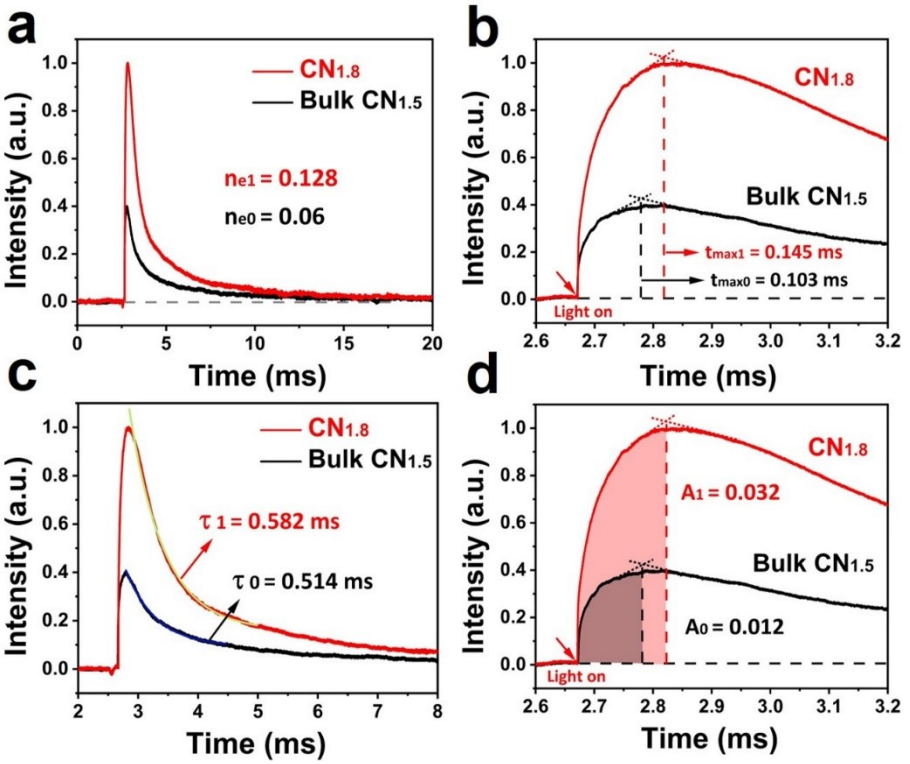

Figure S6. (a) Comparison of the TPV curves with $CN_{1.8}$ and bulk $CN_{1.5}$. (b) Maximum transfer rate of charge of $CN_{1.8}$ and bulk $CN_{1.5}$. (c) Charge recombination process of $CN_{1.8}$ and bulk $CN_{1.5}$. (d) Charge extraction process of $CN_{1.8}$ and bulk $CN_{1.5}$.

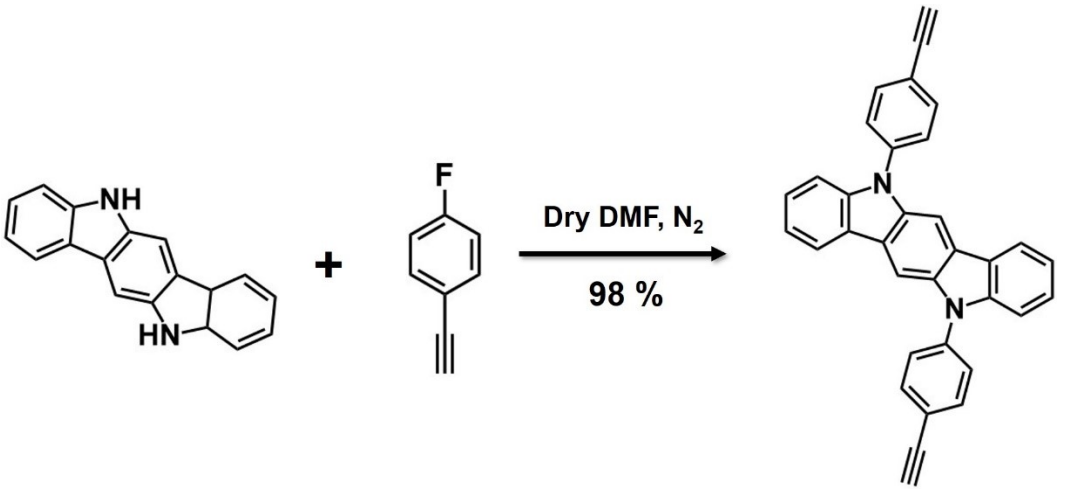

Figure S7. Synthesis route of ICT.

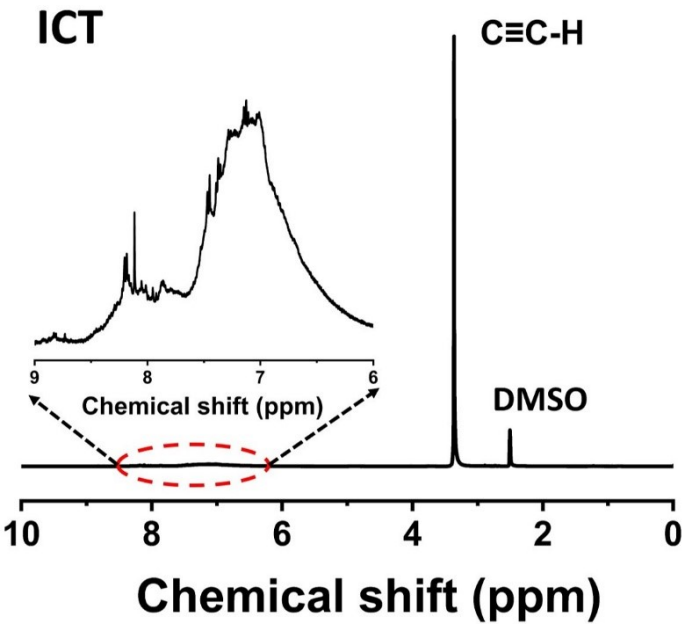

Figure S8. ^{1}H NMR spectrum of the ICT.

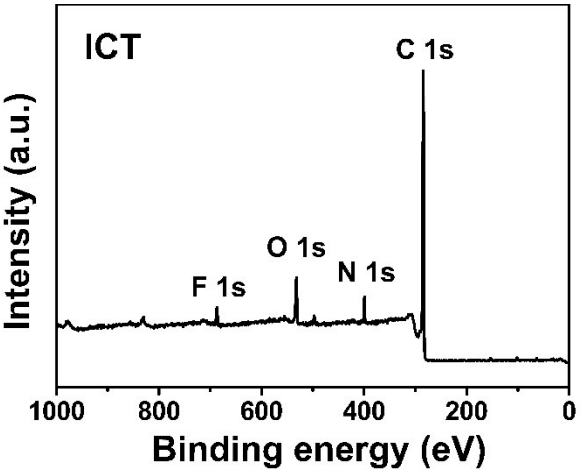

Figure S9. XPS survey spectrum of ICT.

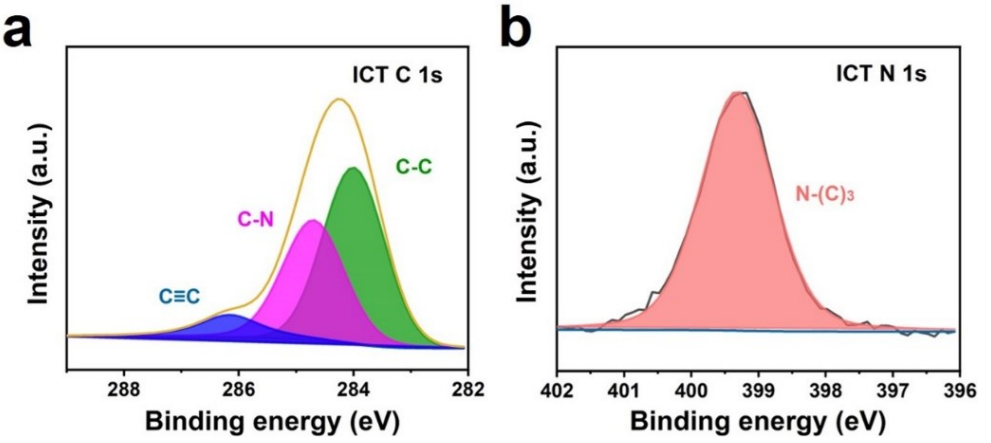

Figure S10. High-resolution XPS spectra of ICT: (a) C 1s, (b) N 1s.

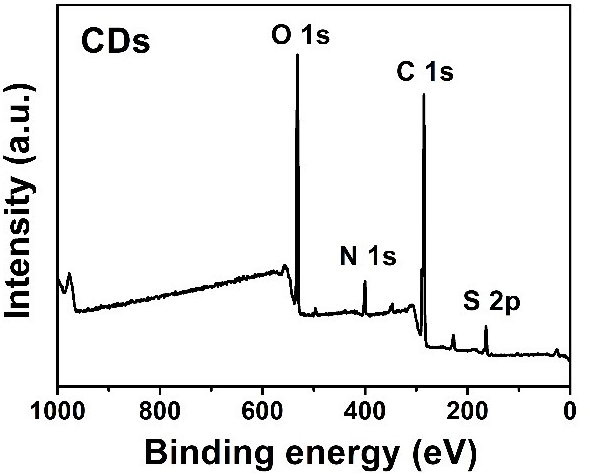

Figure S11. XPS survey spectrum of CDs.

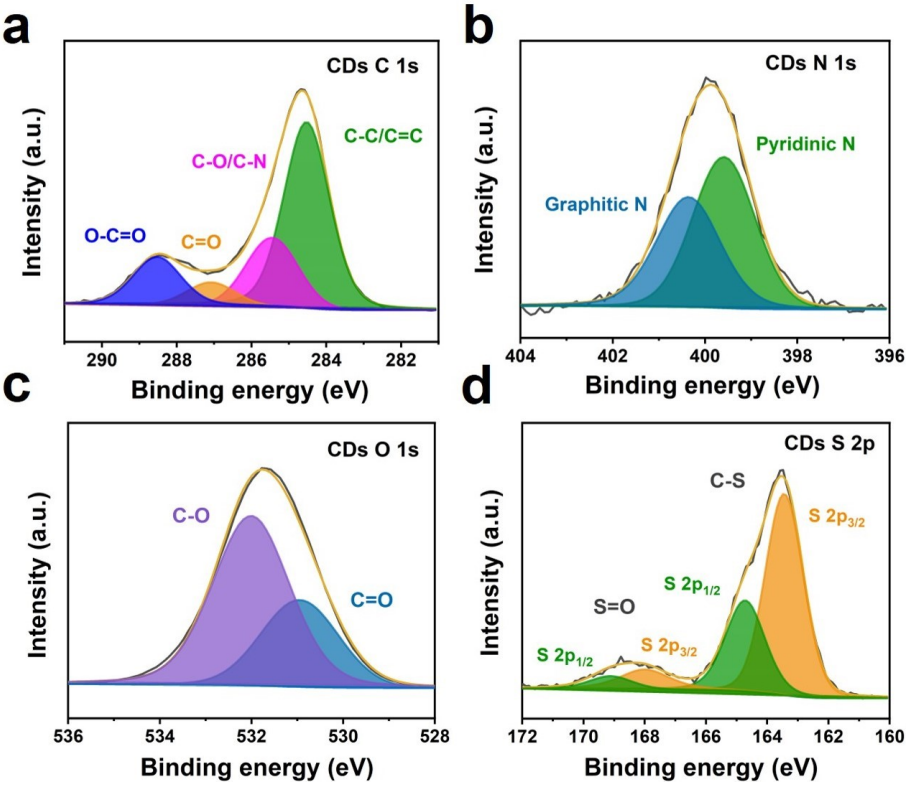

Figure S12. High-resolution XPS spectra of CDs: (a) C 1s, (b) N 1s, (c) O 1s, (d) S 2p.

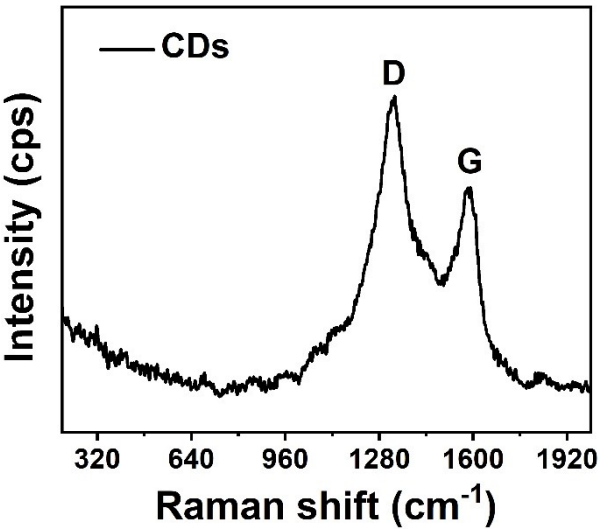

Figure S13. Raman spectra of CDs.

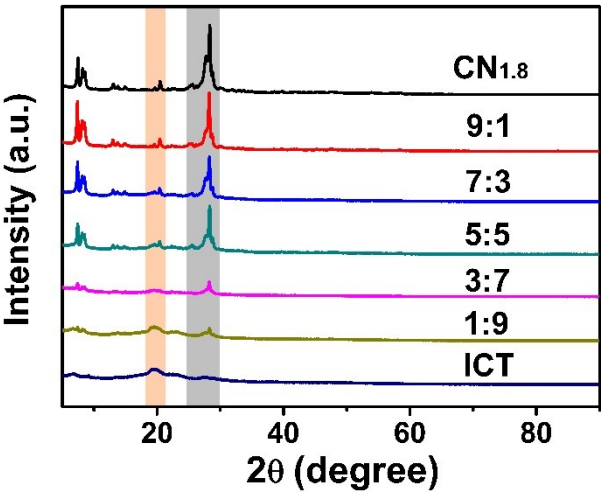

Figure S14. XRD patterns of different $CN_{1.8}$/ICT mass ratios.

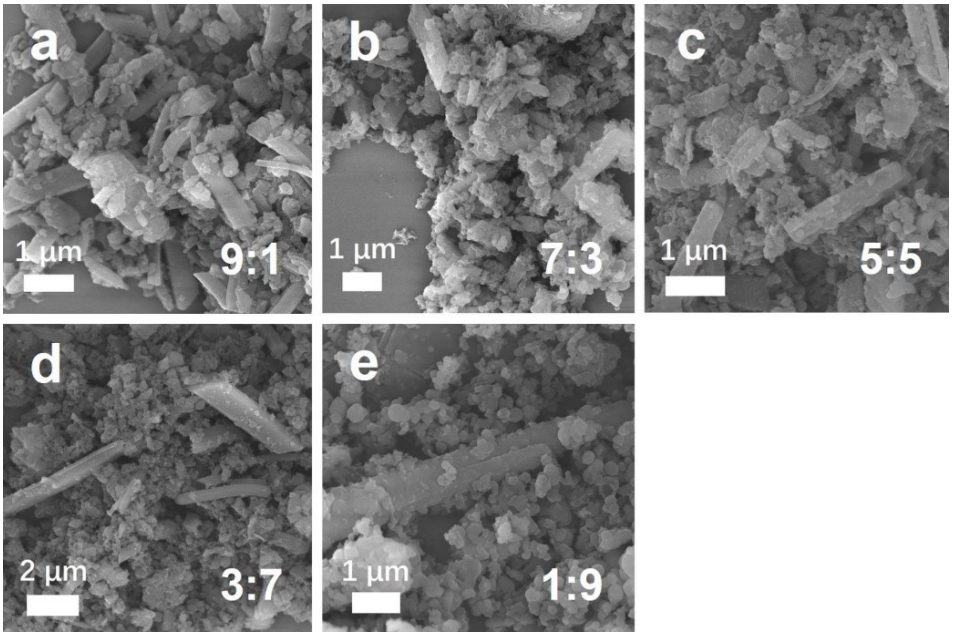

Figure S15. SEM images of different $CN_{1.8}$/ICT mass ratios.

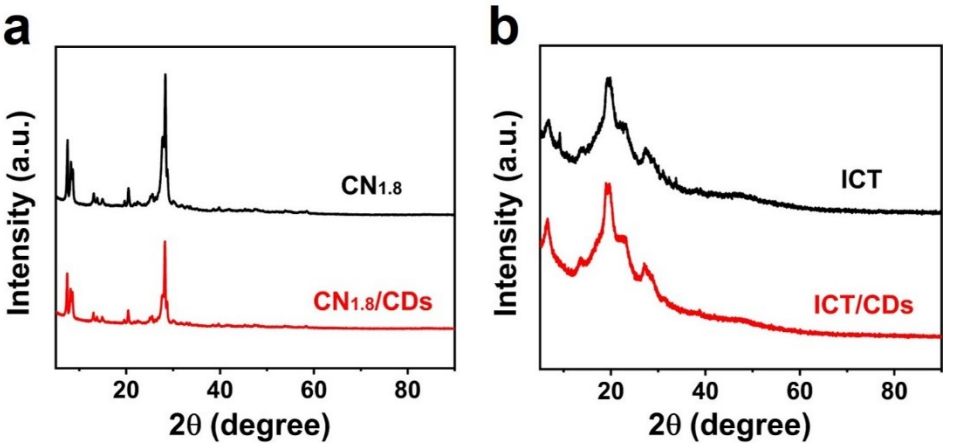

Figure S16. (a) XRD patterns of $CN_{1.8}$ and $CN_{1.8}$/CDs. (b) XRD patterns of ICT and ICT/CDs.

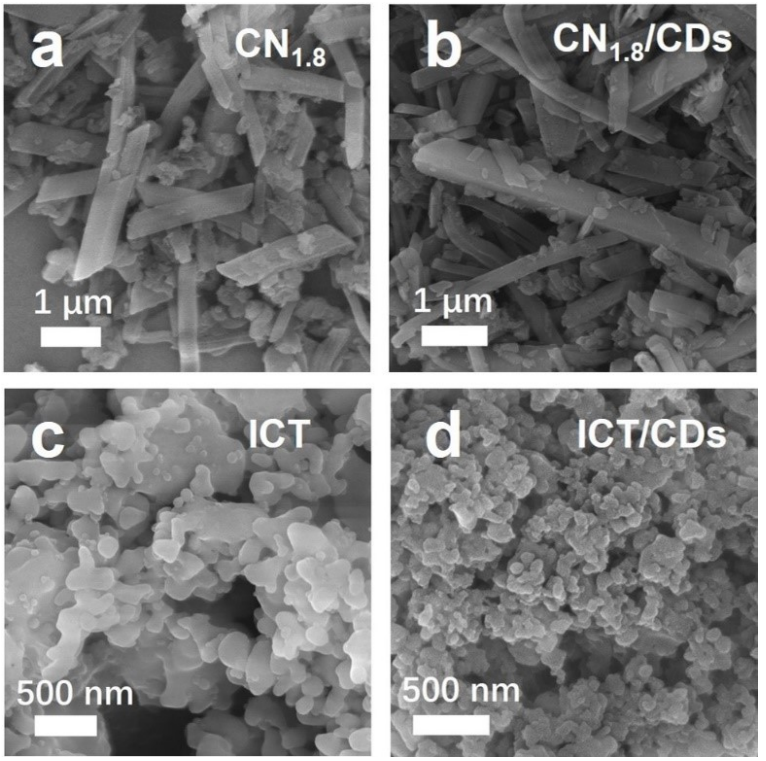

Figure S17. SEM images of (a) $CN_{1.8}$, (b) $CN_{1.8}$/CDs, (c) ICT, and (d) ICT/CDs.

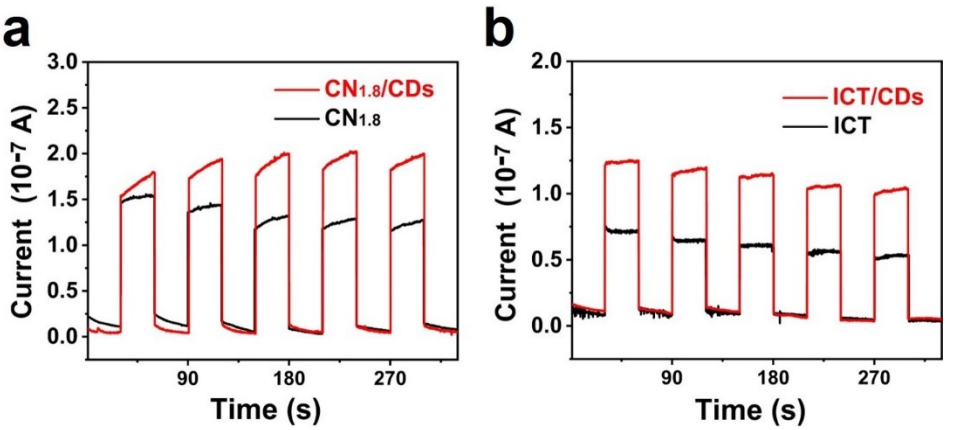

Figure S18. (a) The photocurrent curves of $CN_{1.8}$ and $CN_{1.8}$/CDs. (b) The photocurrent curves of ICT and ICT/CDs (Conditions: under room temperature (0.1 M Na_2SO_4) with indium-tin oxide (ITO) glass ($1\,cm \times 2\,cm$) as the working electrode).

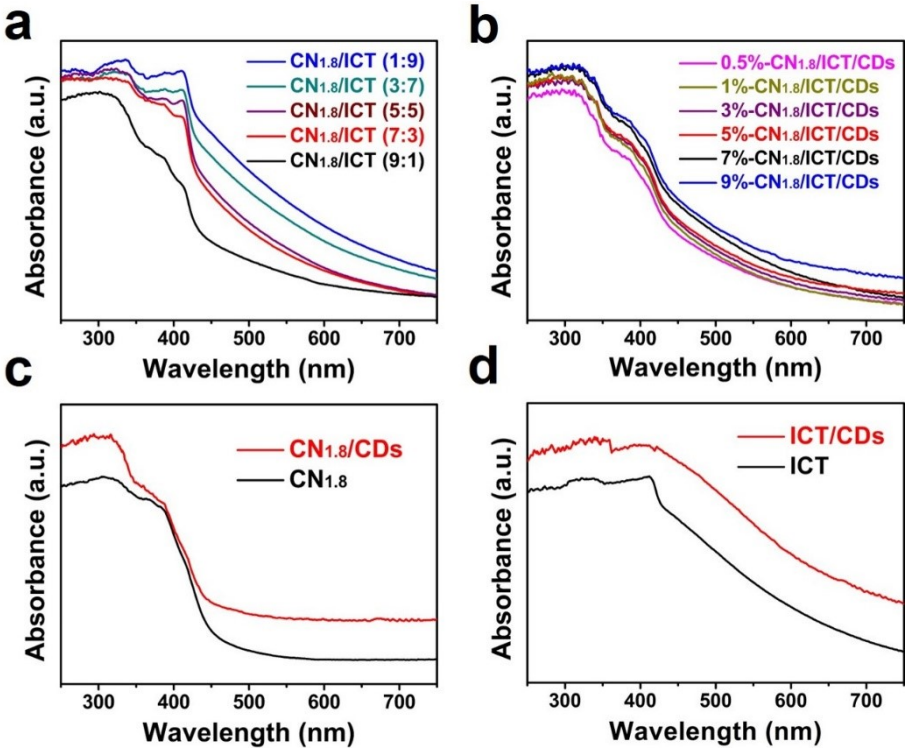

Figure S19. UV-vis absorption spectra of (a) different $CN_{1.8}$/ICT mass ratios, (b) $CN_{1.8}$/ICT/CDs with different concentrations of CDs, (c) $CN_{1.8}$ and $CN_{1.8}$/CDs, and (d) ICT and ICT/CDs.

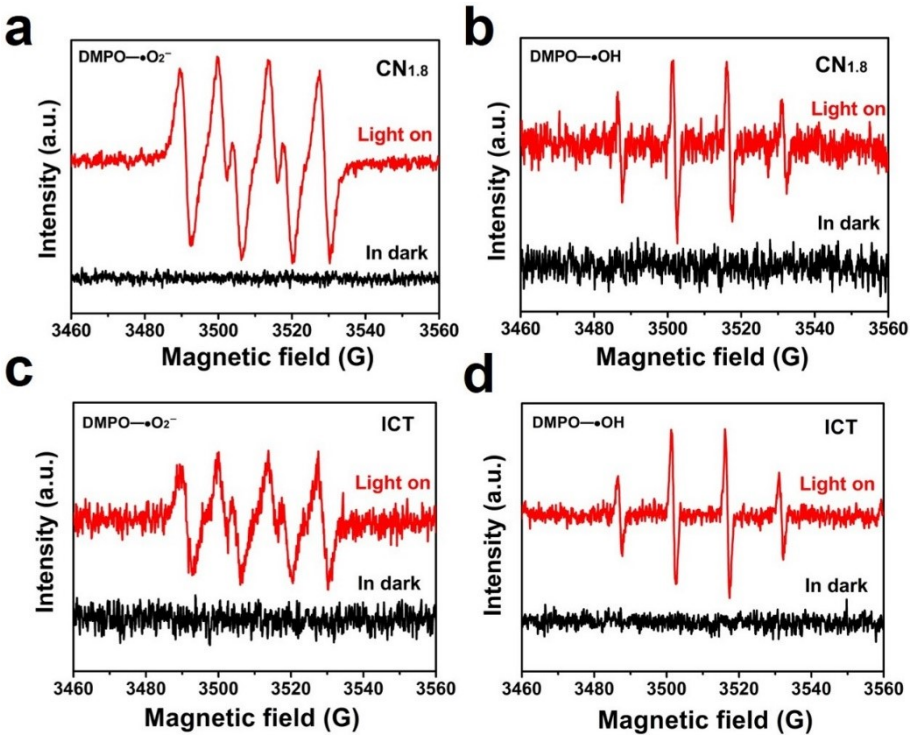

Figure S20. EPR spectra of $CN_{1.8}$ under darkness and light, measuring the presences of (a) $\cdot O_2^-$ and (b) ·OH. EPR spectra of ICT under darkness and light, measuring the presences of (c) $\cdot O_2^-$ and (d) ·OH.

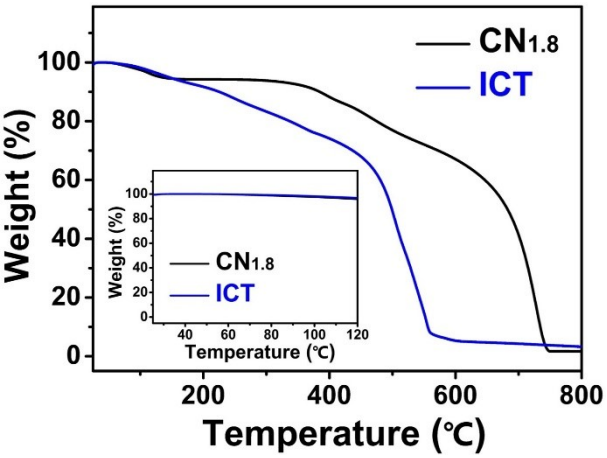

Figure S21. The TGA curves of $CN_{1.8}$ and ICT in the temperature range from 25 ℃ to 800 ℃ (inserted picture: The TGA curves of $CN_{1.8}$ and ICT in the temperature range from 25 ℃ to 120 ℃).

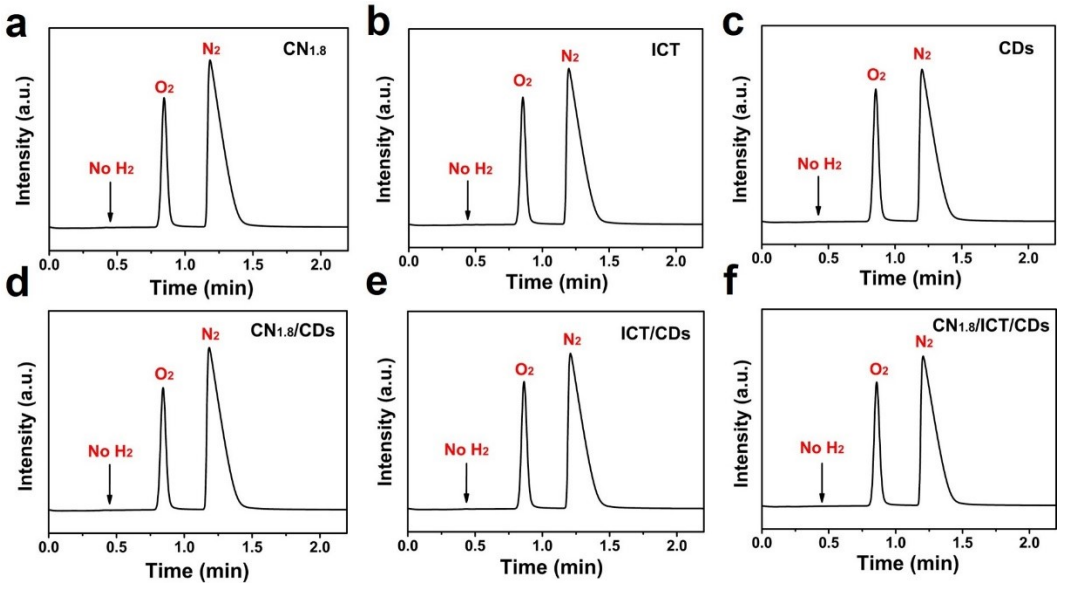

Figure S22. Detection of H_2 with different samples by Gas chromatograph (GC-4000 A). There is no H_2 produced when any sample was used as photocatalyst. (8 mg photocatalyst, 15 mL H_2O, air atmosphere, visible light irradiation for 24 h, light intensity: 95.0 mW cm^{-2}.

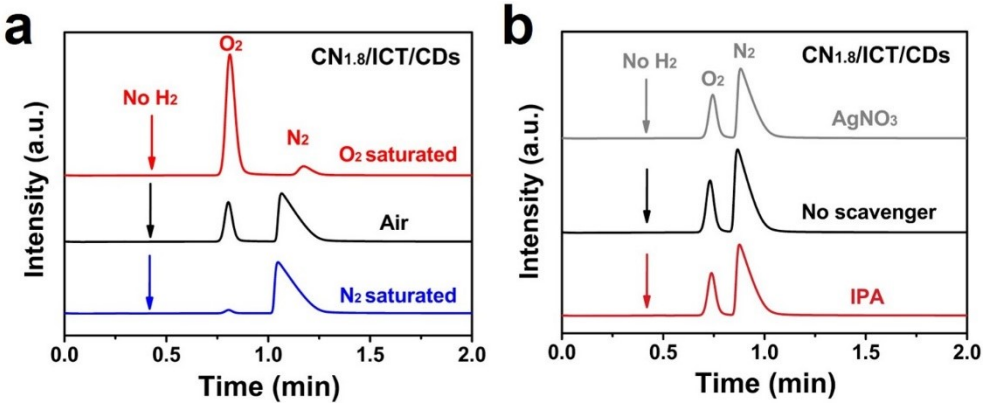

Figure S23. Detection of H_2 of $CN_{1.8}$/ICT/CDs at (a) different atmospheres (N_2/Air/O_2) and (b) different scavenger ($AgNO_3$/No Scavenger/IPA) by Gas chromatograph (GC-4000 A). There is no H_2 produced at all conditions when $CN_{1.8}$/ICT/CDs was used as photocatalyst. (8 mg photocatalyst, 15 mL H_2O, visible light irradiation for 6 h, light intensity: 95.0 mW cm^{-2}).

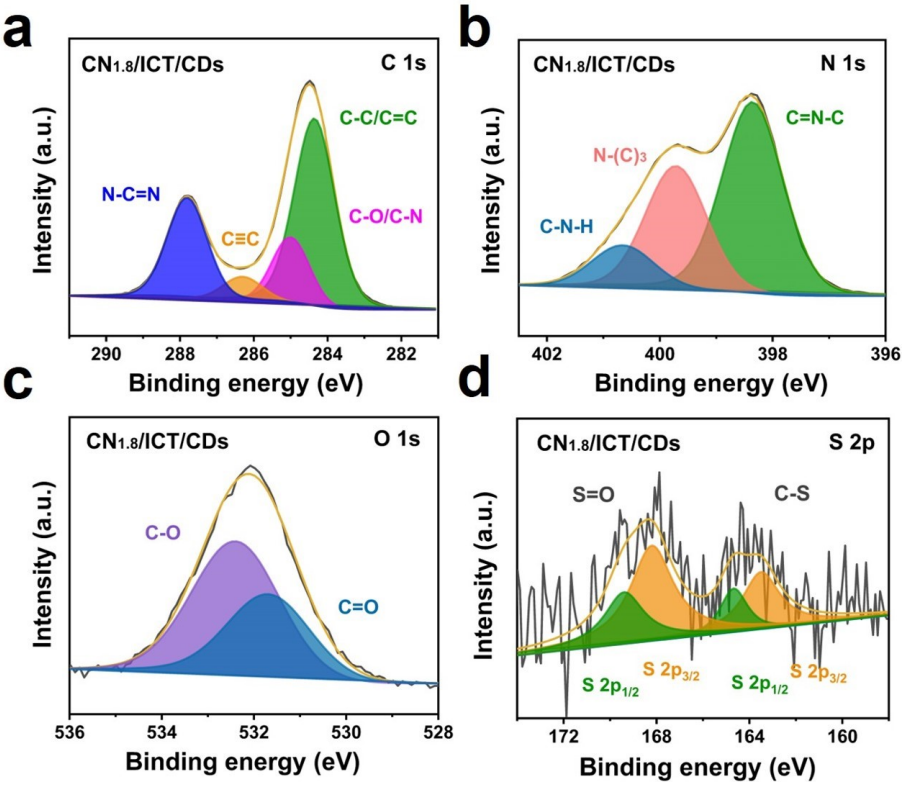

Figure S24. High-resolution XPS spectra of $CN_{1.8}$/ICT/CDs: (a) C 1s, (b) N 1s, (c) O 1s, (d) S 2p.

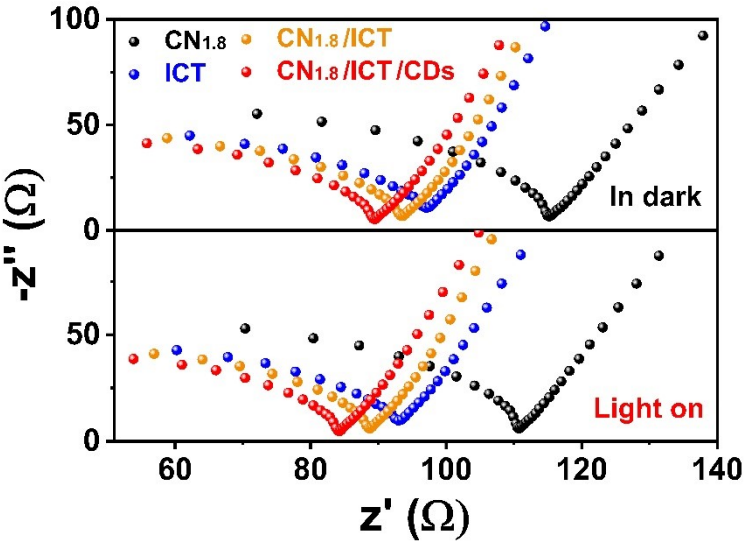

Figure S25. The EIS curves of $CN_{1.8}$, ICT, $CN_{1.8}$/ICT and $CN_{1.8}$/ICT/CDs under light-on and light-off with glassy carbon electrode as the working electrode.

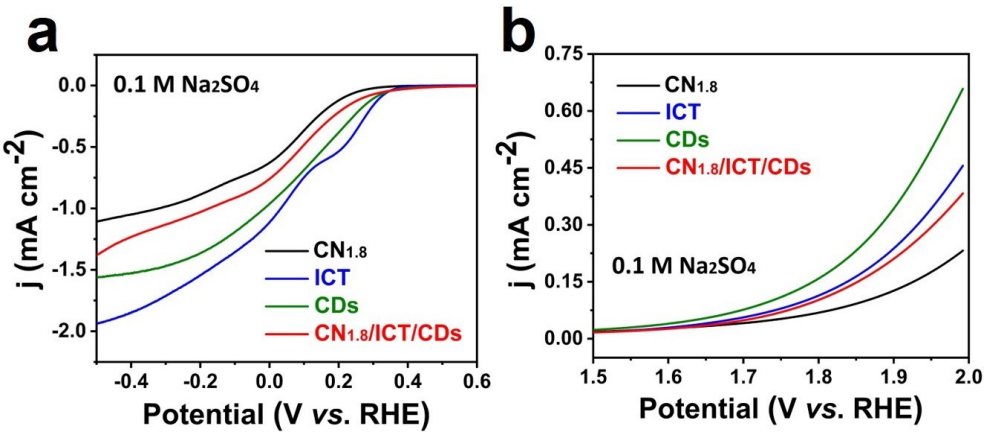

Figure S26. (a) ORR performance of $CN_{1.8}$, ICT, CDs and $CN_{1.8}$/ICT/CDs in O_2 saturation (0.1 M Na_2SO_4) with the rate of 1600 rpm. (b) OER performance of $CN_{1.8}$, ICT, CDs and $CN_{1.8}$/ICT/CDs (0.1 M Na_2SO_4).

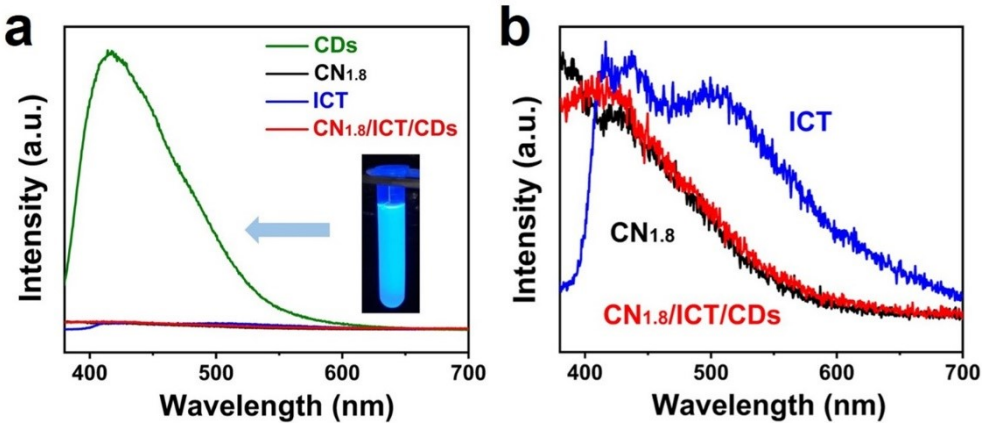

Figure S27. (a) The photoluminescence (PL) spectra of CDs, $CN_{1.8}$, ICT and $CN_{1.8}$/ICT/CDs (inserted picture: the photograph of CDs solution excited by UV lamp at 365 nm). (b) The PL spectra of $CN_{1.8}$, ICT and $CN_{1.8}$/ICT/CDs in larger version.

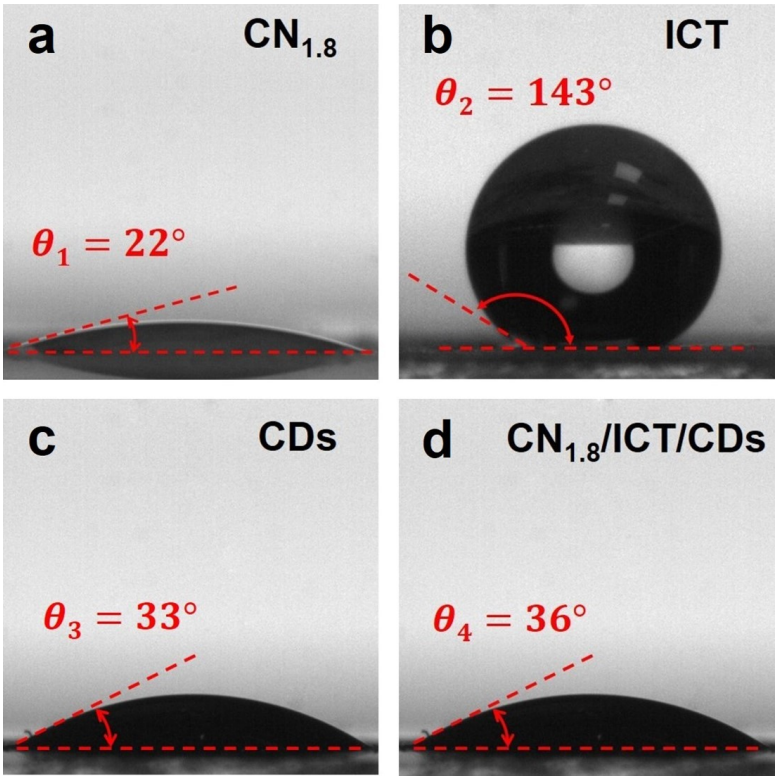

Figure S28. The contact angle images of water droplets on the surface of (a) $CN_{1.8}$, (b) ICT, (c) CDs and (d) $CN_{1.8}$/ICT/CDs. The surface of the material is hydrophilic ($\theta \leq 90°$), and the surface of the material is hydrophobic ($\theta > 90°$).

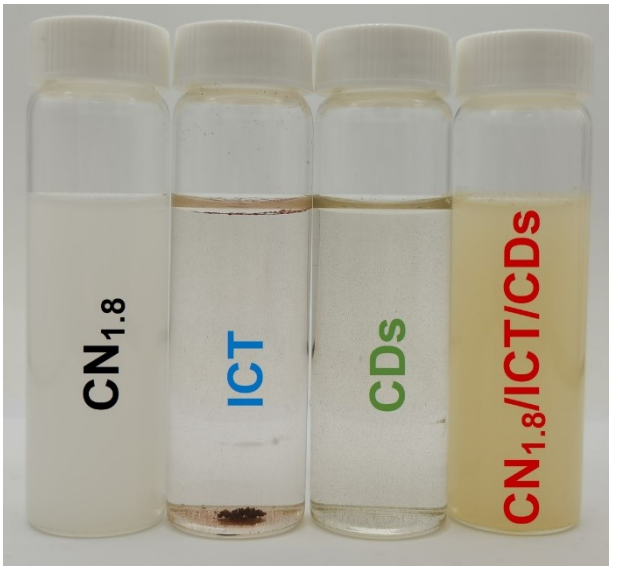

Figure S29. The water-soluble images of $CN_{1.8}$, ICT, CDs and $CN_{1.8}$/ICT/CDs.

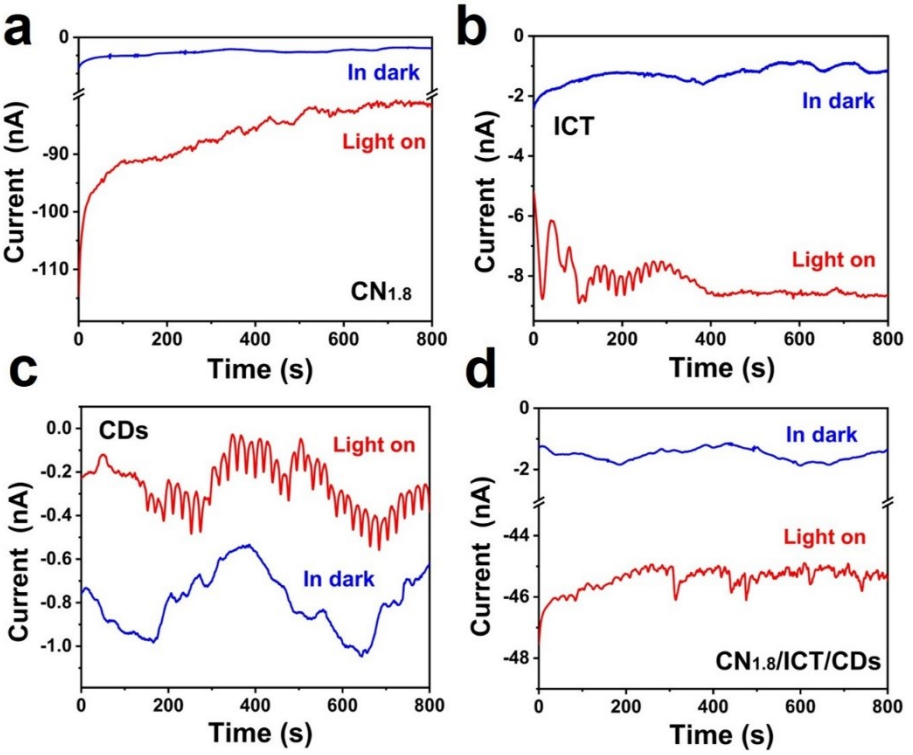

Figure S30. The current-time curve of (a) $CN_{1.8}$, (b) ICT, (c) CDs and (d) $CN_{1.8}$/ICT/CDs with light-off and light-on.

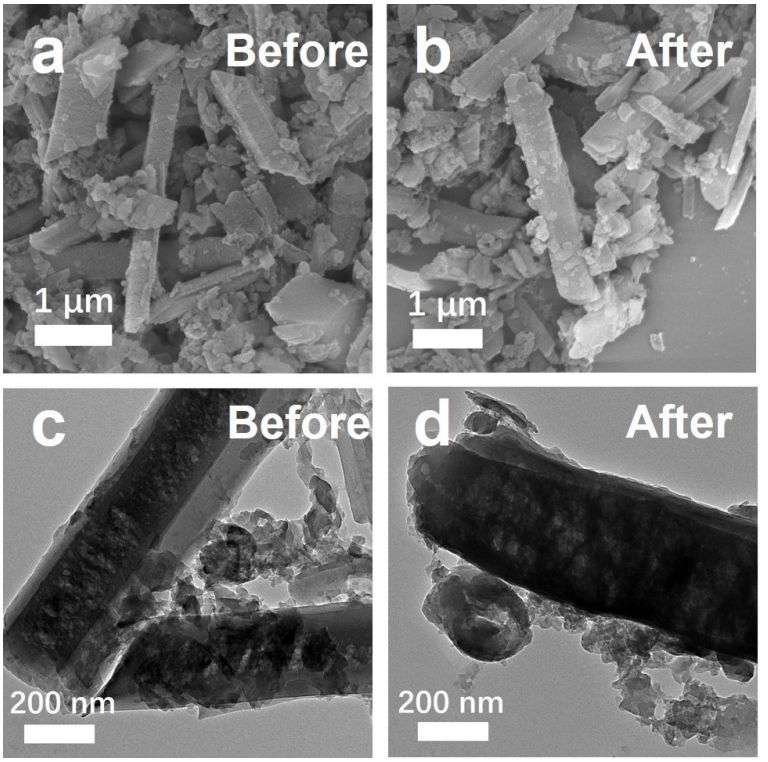

Figure S31. The SEM images of $CN_{1.8}$/ICT/CDs (a) before and (b) after five photocatalytic test cycles. The TEM images of $CN_{1.8}$/ICT/CDs (c) before and (d) after five photocatalytic test cycles.

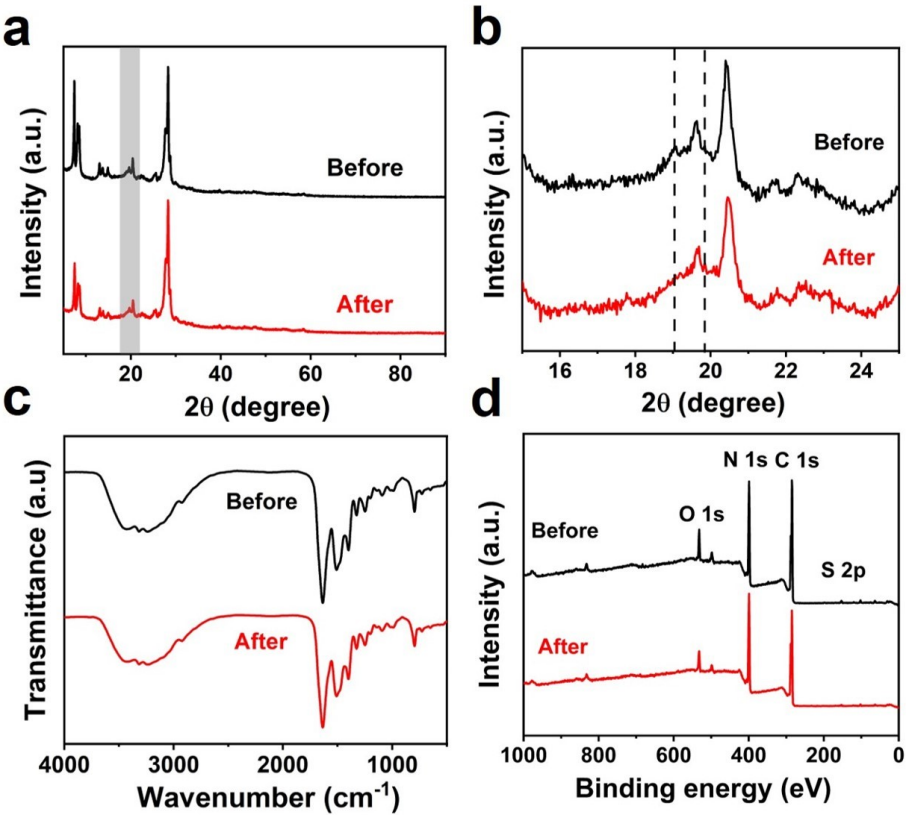

Figure S32. (a-b) XRD patterns of $CN_{1.8}$/ICT/CDs before and after five photocatalytic test cycles. (c) FTIR spectra and (d) XPS survey spectrum of $CN_{1.8}$/ICT/CDs before and after five photocatalytic test cycles

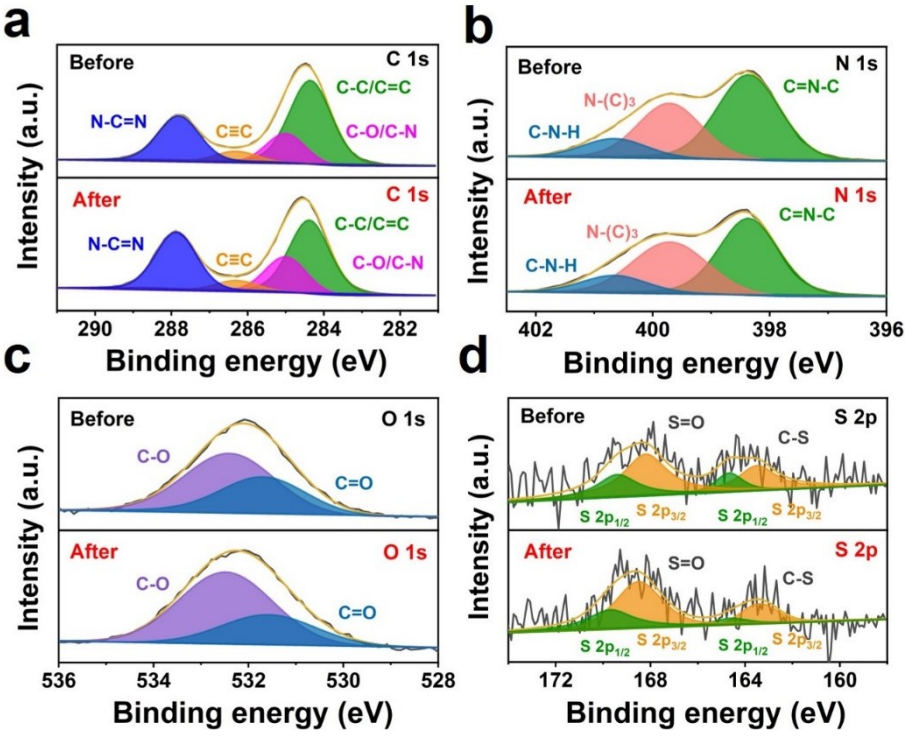

Figure S33. High-resolution XPS spectra of $CN_{1.8}$/ICT/CDs after five photocatalytic test cycles: (a) C 1s, (b) N 1s, (c) O 1s and (d) S 2p.

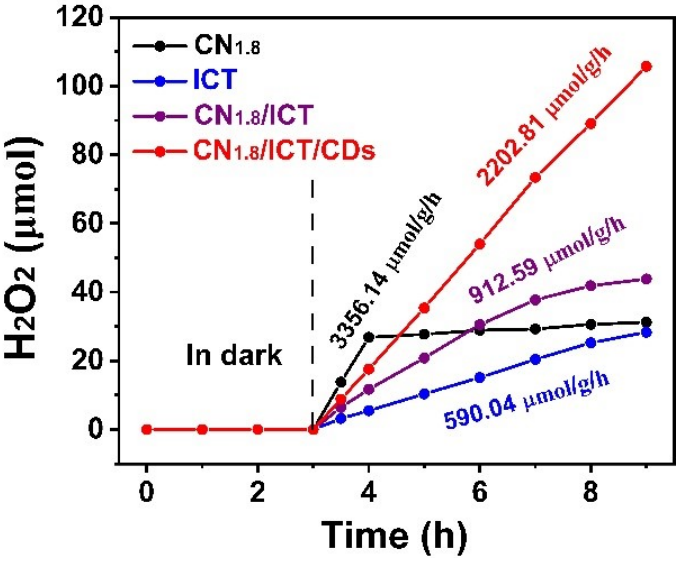

Figure S34. Evolution of H_2O_2 catalyzed by $CN_{1.8}$, ICT, $CN_{1.8}$/ICT, and $CN_{1.8}$/ICT/CDs under light-on and in dark.

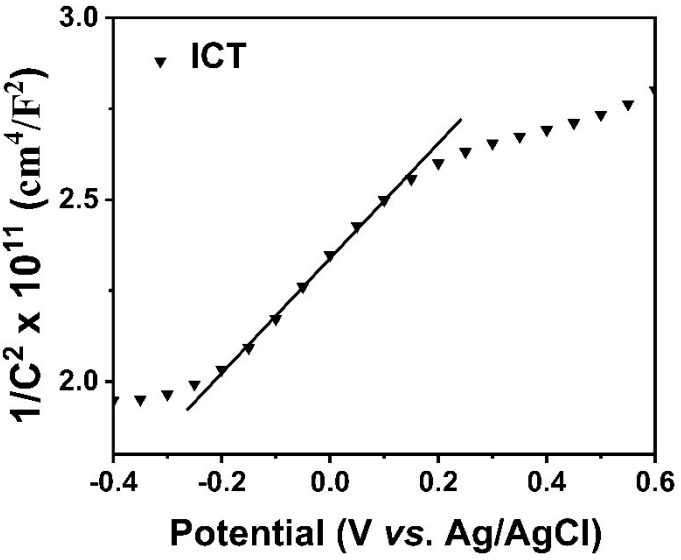

Figure S35. The Mott-Schottky plots of ICT.

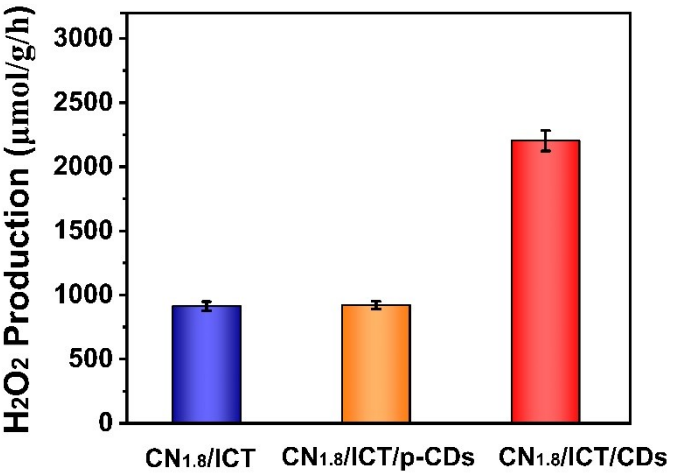

Figure S36. Comparison of H_2O_2 evolution produced by $CN_{1.8}$/ICT, $CN_{1.8}$/ICT/p-CDs and $CN_{1.8}$/ICT/CDs.

Preparation of pristine CDs: pristine CDs were synthesized by the one-step hydrothermal method. Simply, 192.13 mg (1 mmol) citric acid was mixed with 50 mL deionized water and then stirred for 30 mins. The mixture was heated at 220 °C for 6 h. After cooling down, the mixture solution was filtered with 0.22 μm filter to remove the large particles. Then, dialyzed in deionized water through a 1000 Dalton dialysis bag for 48 h, and the ultrapure water was replaced every 4 h to remove precursors and byproducts. Finally, pristine CDs powder was obtained after removing the water. The sample was named p-CDs.

Tables

Table S3. A survey and comparison of the photocatalytic H_2O_2 production performance from our and the currently reported works.

Catalyst	Light	Scavenger	Solution	H_2O_2 Production (μmol/h/g)	AQE	Cycle	Ref.
$CN_{1.8}$/ICT/CDs	**λ>420 nm**	**/**	**Water**	**2202.81**	**12.65**	**5**	**This work**
Au/$BiVO_4$	λ>420 nm	EtOH/ $AgNO_3$	O_2 water	2.412	0.24%	/	1
rGO/$Cd_3(TMT)_2$	λ>420 nm	methanol	O_2 water	109.4	6.8% (450 nm)	/	2
CN nanotubes	simulated sunlight	/	O_2 water	240.36	/	6	3
CPN	λ>420 nm	/	Water	1968	1.57%	6	4
PM-CDs-30	λ>420 nm	/	Real seawater	1776	1.1%	5	5
g-C_3N_4/$NaBH_4$	λ>420 nm	/	Water	170	4.3%	4	6
Cv-g-C_3N_4	λ>420 nm	/	Water	95±5	/	4	7
PI_x-NCN	λ>420nm	/	Water	1200	3.2%	10	8
OCN-500	λ>420 nm	isopropanol alcohol	O_2 water	2920	10.2%	4	9
g-C_3N_4/BDI	λ>420 nm	/	O_2 water	9.7	2.6%	/	10
g-C_3N_4/PI/rGO	λ>420 nm	/	Water	900±50	/	3	11
g-C_3N_4	λ>420 nm	EtOH	O_2 water	125	12%	/	12
g-C_3N_4/PDIx	λ>420 nm	/	O_2 water	12.5	/	/	13
BP/g-C_3N_4	λ>420 nm	isopropanol	O_2 water	540	/	10	14
g-C_3N_4-CNTs	λ≥400 nm	Formic acid	O_2 water	326	/	3	15

References

1. H. Hirakawa, S. Shiota, Y. Shiraishi, H. Sakamoto, S. Ichikawa and T. Hirai, *ACS Catal*. 2016, **6**, 4976–4982.
2. J. Xu, Z. Chen, H. Zhang, G. Lin, H. Lin a, X. Wang and J. Long, *Sci. Bull.,* 2017, **62**, 610–618.
3. L. Zhou, J. Lei, F. Wang, L. Wang, M. R. Hoffmann, Y. Liu, S.-I. In and J. Zhang, *Appl. Catal., B*, 2021, **288**, 119993.
4. J. Cao, H. Wang, Y. Zhao, Y. Liu, Q. Wu, H. Huang, M. Shao, Y. Liu and Z. Kang, *J. Mater. Chem. A*, 2020, **8**, 3701-3707.
5. Q. Wu, J. Cao, X. Wang, Y. Liu, Y. Zhao, H. Wang, Y. Liu, H. Huang, F. Liao, M. Shao and Z. Kang, *Nat. Commun.*, 2021, **12**, 483.
6. Z. Zhu, H. Pan, M. Murugananthan, J. Gong and Y. Zhang, *Appl. Catal. B Environ.,* 2018, **232**, 19–25.
7. S. Li, G. Dong, R. Haililim, L. Yang, Y. Li, F. Wang, Y. Zeng and C. Wang, *Appl. Catal. B Environ.,* 2016, **190**, 26–35.
8. L. Yang, G. Dong , D. Jacobs, Y. Wang, L. Zang and C. Wang, *J. Catal.,* 2017, **352**, 274–281.
9. Z. Wei, M. Liu, Z. Zhang, W. Yao, H. Tan and Y. Zhu, *Energy Environ. Sci.,* 2018, **11**, 2581–2589.
10. Y. Kofuji, S. Ohkita, Y. Shiraishi, H. Sakamoto, S. Tanaka, S. Ichikawa and T. Hirai, *ACS Catal.,* 2016, **6**, 7021–7029.

11. L. Yang, P. Wang, J. Yin, C. Wang, G. Dong, Y. Wang and W. Ho, *Appl. Catal. B Environ.,* 2019, **250**, 42–51.

12. Y. Shiraishi, S. Kanazawa, Y. Sugano, D. Tsukamoto, H. Sakamoto, S. Ichikawa and T. Hirai, *ACS Catal.,* 2014, **4**, 774–780.

13. Y. Shiraishi, S. Kanazawa, Y. Kofuji, H. Sakamoto, S. Ichikawa, S. Tanaka and T. Harai, *Angew. Chem. Int. Ed.,* 2014, **53**, 13454–13459.

14. Y. Zheng, Z. Yu, H. Ou, A. Asiri, Y. Chen and X. Wang, *Adv. Funct. Mater.,* 2018, **28**, 1705407.

15. S. Zhao, T. Guo, X. Li, T. Xu, B. Yang and X. Zhao, *Appl. Catal. B Environ*., 2018, **224**, 725–732.